Molecular Crystals and Liquid Crystals

Publication details, including instructions for authors and subscription information:
http://www.tandfonline.com/loi/gmcl20

Structure of Latent Heavy Ion Tracks in Polyimide

Sameer Abu Saleh [a] & Yehuda Eyal [a]

[a] Department of Chemistry, Technion-Israel Institute of Technology, Haifa, Israel

Version of record first published: 31 Jan 2007

To cite this article: Sameer Abu Saleh & Yehuda Eyal (2006): Structure of Latent Heavy Ion Tracks in Polyimide, Molecular Crystals and Liquid Crystals, 448:1, 233/[835]-242/[844]

To link to this article: http://dx.doi.org/10.1080/15421400500402798

Mol. Cryst. Liq. Cryst., Vol. 448, pp. 233/[835]–242/[844], 2006

ISSN: 1542-1406 print/1563-5287 online
DOI: 10.1080/15421400500402798

Taylor & Francis
Taylor & Francis Group

Structure of Latent Heavy Ion Tracks in Polyimide

Sameer Abu Saleh
Yehuda Eyal
Department of Chemistry, Technion–Israel Institute of Technology, Haifa, Israel

Employing small-angle X-ray scattering, we have confirmed that tracks along wakes of GeV heavy ions in polyimide possess a porous structure. Moreover, specific free volume of ~20 nm^3 per nm of track length, independent of track length, has been revealed along 5.5-nm-diameter 25 to 125 μm long tracks created by 2.19 GeV Au ions. Structural alteration involves, undoubtedly, highly-efficient material expulsion, and is attributed to a confined ion-induced radiolysis followed by removal of gaseous and volatile degradation products, most likely through the low-density tracks. Porosity enables selective track etching, doping, coating, or filling, which make tracks useful for nanotechnological applications.

Keywords: ion tracks; polyimide; SAXS; swift heavy ions; track structure

PACS: 61.10.Eq; 61.80.Jh; 78.55.Fv

1. INTRODUCTION

Energetic heavy ions that move through an insulating solid create nanometric wide ion damage trails, *latent ion track*s, along their paths. Polymeric ion tracks exhibit highly elevated chemical reactivity relative to the reactivity of the surrounding intact matrix [1,2]. As a result, these tracks can undergo a series of selective treatments, e.g., etching, radial enlargement, doping, coating and filling. Although fundamental track characteristics such as longitudinal and radial

The authors thank C. Trautmann, GSI, Darmstadt, for performing the irradiations of the polyimide foils and for valuable suggestions. This work was supported by grant 23/03 of the Israel Science Foundation, and by the S. Langberg Nuclear Research Fund at the Technion.

Address correspondence to Yehuda Eyal, Department of Chemistry, Technion–Israel Institute of Technology, Haifa 32000, Israel. E-mail: cheyal@techunix.technion.ac.il

structure and longitudinal and radial chemical composition are largely scarce, ion tracks have proven attractive containment and template structures for fabrication of materials and devices of nanoscopic width (see, e.g., Refs. [3–6]).

The pronounced etchability of polymeric ion tracks has long been attributed to chemically-reactive alteration products such as trapped electrons, ions, radicals, and molecular fragments. Recently, additional influence by significant ion-induced porosity has been suggested [7,8]. In-track free volume should accelerate etching by increasing the contact area between residual damaged material and permeating etchants.

As revealed by small-angle X-ray scattering (SAXS), cores of 10-year old tracks created by 2.64 GeV U ions through 50 and 60 μm thick polyimide and polycarbonate foils are ~5.8-nm diameter largely-hard cylinders with specific free volumes of ~17 and ~18 nm^3 per nm of track length, respectively [7,8]. The tracks in each of these two substrates were formed under nearly uniform ion linear energy transfer (LET), and model analyses have suggested that the resulting porosity is uniform as well along the track cores [7,8]. Obviously, empirical verification of this useful track characteristic is warranted.

Employing SAXS, we report structure parameters of tracks with lengths ranging from 25 to 125 μm, created by penetrating 2.19 GeV Au ions through polyimide foils. Polyimide is a promising substrate for track applications [9] due to its excellent mechanical, chemical, thermal, and radiation resistance.

2. SPECIMENS AND PROCEDURES

The specimens employed were 25, 50, 75, and 125 μm thick polypyromellitimide foils (DuPont trade name *kapton*, repeat unit $H_{10}C_{22}N_2O_5$, density 1.43 g/cm^3). Ion irradiations were performed at GSI, Darmstadt, 4 months prior to the present SAXS study. Samples were irradiated *in vacuo* with penetrating 2.19 GeV Au ions at normal incidence. Thus, the track length, L, is given by the foil thickness. Because severity of ion-induced damage is expected to depend upon the local ion LET, we have assured as much as possible track creation under similar LET in all samples, independent of the track length. Therefore, we irradiated and examined four samples as follows: A stack of 4×25-μm thick foils and a stack of 2×50-μm thick foils (mean LET and dispersion in each sample 15.6 ± 0.7 keV/nm), a single foil 75 μm thick (LET 15.3 ± 0.7 keV/nm), and a single foil 125 μm thick (LET 15.7 ± 0.7 keV/nm). After irradiation, the

samples were kept under normal room conditions, mostly in the dark. The track areal density, determined by brief track etching combined with high-resolution scanning electron microscopy [10], was $5.2 \times 10^{10}\,\mathrm{cm}^{-2}$ ($\pm 3\%$).

The SAXS measurements were carried out as described in Refs. [7] and [8]. Briefly, we employed an $\sim$100-μm diameter Cu K_α X-ray beam and a 1024×1024 pixel X-ray detector. The detector covered polar, θ, and azimuthal, ϕ, scattering angles from ~ 0.2 to 4.5° and from 0 to 360°, respectively. The track-originated SAXS yield was obtained by correcting the observed yield for contributions of intact polymer, instrumental background X radiation, and detector noise. We have neglected interference effects due to 6% track overlap, evaluated [11] from the track diameter extracted in the SAXS analysis and from the measured areal density of the tracks. Thus, the SAXS intensity was interpreted as the incoherent sum of intensities of individual tracks.

The product of the X-ray beam intensity on target and the intrinsic detector efficiency was calibrated by scattering on water (uncertainty 5%) [7,8], and the stability of this product over time was ensured by frequently monitoring the yield of X-rays scattered by a reference carbon glass target. Knowledge of this product enabled us to derive absolute SAXS cross sections.

3. RESULTS

The SAXS measurements were conducted with samples tilted away vertically by an angle $\beta = 30^\circ$ from the axis of the primary X-ray beam. All observed two-dimensional scattering patterns exhibited high angular anisotropy, as shown for the ion-irradiated 75-μm thick polyimide foil in Figure 1. This feature clearly indicates the importance of modified density all along the ion wake. Simulation of the experiments (see the following) has indicated that all registered track-originated SAXS events reside in the two mirror-like streaks that extend outward from the center of the X-ray detector and limited to narrow intervals of ϕ (see Fig. 1). Each of these events is characterized by $q_r = q$ or $q_r \sim q$ and $q_z = 0$ or $q_z \sim 0$, respectively, where $q = (4\pi/\lambda)\sin(\theta/2)$ is the modulus of the scattering vector in the reciprocal space, and q_r and q_z are the components of q perpendicular and parallel to the track axis, respectively. Therefore, following the analysis procedure described in Ref. [7], the empirical two-dimensional SAXS yields (Fig. 1) were conveniently translated to one-dimensional yields. Specifically, track-originated scattering

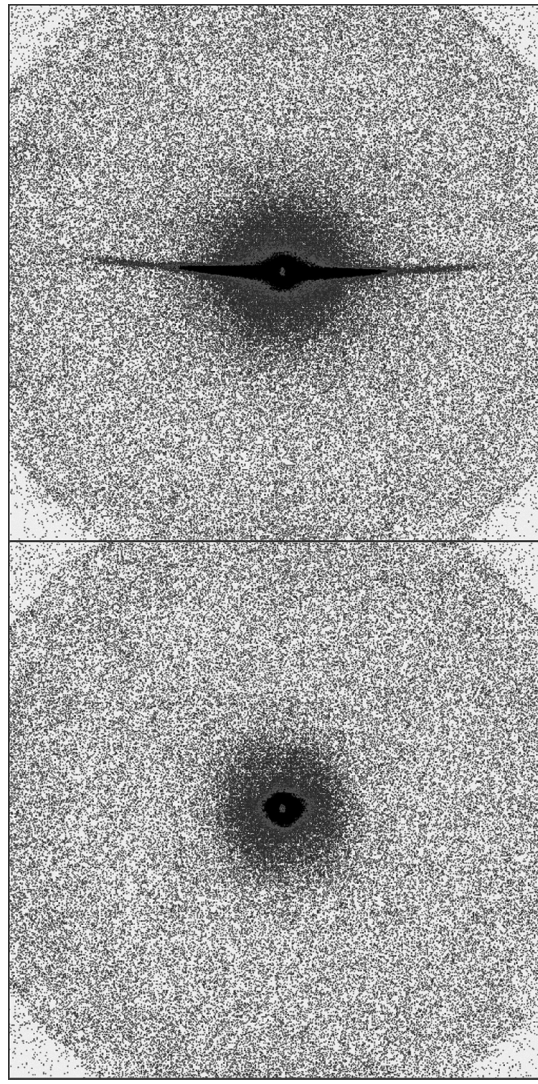

FIGURE 1 SAXS patterns generated by 75-μm thick polyimide foils. The foils were tilted vertically by 30° relative to the direction of the primary X-ray beam. Upper panel – scattering by a foil containing tracks created by 2.19 GeV Au ions; lower panel – scattering by a control unirradiated foil.

events, at pixel-wide intervals of θ, were integrated over ϕ across the streak. These one-dimensional yields were then divided by the number of foils in the irradiated sample to yield track-length-dependent

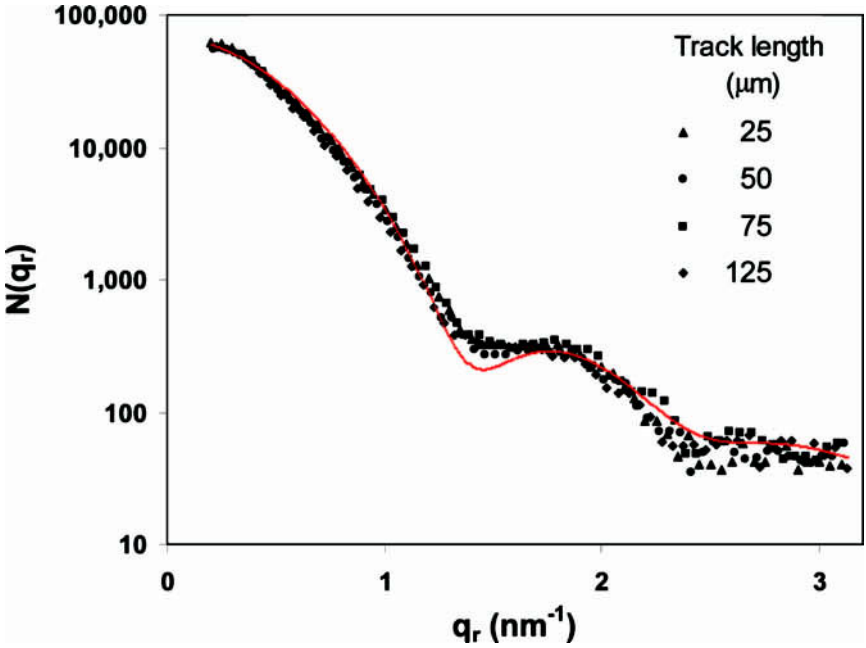

FIGURE 2 A composite display of unidimensional SAXS yields, $N(q_r)$, obtained by adjustment of empirical yields generated by tracks 25, 50, 75, and 125 μm long to yields expected from scattering on 100-μm long tracks in experiments that last 45 hours (see text). The quantity q_r is the modulus of the radial component of the scattering vector in the reciprocal space.

scattering yields, $N_L(q_r)$. Here, the subscript L designates the track length. The four corresponding L-dependant sequences of average experimental track scattering cross sections are given by

$$\sigma_{\mathrm{L,exp}}(q_r) = N_L(q_r)\frac{\cos\beta}{P\varepsilon tD} \tag{1}$$

where $P(\mathrm{s}^{-1})$ is the intensity of the X-ray beam on target, , ε (dimensionless quantity, $0 < \varepsilon < 1$) is the intrinsic detector efficiency, D is the areal density of the tracks, and t is the duration of each SAXS measurement, typically a few tens of hours.

Our experiment shows that within experimental uncertainties, empirical $\sigma_{L,\mathrm{exp}}(q_r)$ values are linearly proportional to L. This feature manifests itself by the well-defined composite yield sequence shown in Figure 2, given by $N(q_r) = N_L(q_r)$ [100/L(μm)] [45/t(h)]. The sequence includes data pertaining to all 4 empirical $N_L(q_r)$ sequences, and

represents yields expected from scattering on 100-μm long tracks in experiments that last 45 hours. It is also evident from Figure 2 that the data exhibit an oscillatory angular distribution.

4. TRACK MODEL AND THEORETICAL SAXS CROSS SECTIONS

As mentioned in Section 3, the observed anisotropic scattering clearly indicates the importance of modified density all along the tracks. Following Ref. [7], we have attributed the SAXS signal to density depletion, because compaction of the polymer under the ion beam can be safely ruled out. The oscillatory scattering yield (see Fig. 2) indicates a rather abrupt change of density at the circumference of the track core. Therefore, we have assumed scattering by a population of depleted columnar structures with largely hard boundaries and cylindrical symmetry. The electron density function was taken to be the same all along the track. Its radial profile, $\rho(r)$, is the sum of contributions of a hard cylinder and a Gaussian with fractional weights s and $1-s$, respectively ($0 \le s \le 1$),

$$\rho(r) = f\rho_o[s\delta + (1-s)\exp(-r^2/R^2)]. \tag{2}$$

The quantity ρ_o is the mean electron density in the polymer matrix, f is the fractional electron density deficit at the track center, R, designated herein as the track radius, is the radial extension of the hard-cylinder component and the e^{-1} radius of the Gaussian component, $\delta = 1$ at $r \le R$ and $\delta = 0$ at $r > R$.

Two-dimensional SAXS amplitudes of a hard cylinder have been derived in Ref. [12]. Two-dimensional scattering amplitudes and two-dimensional scattering intensities of a tilted model track with a pure Gaussian radial electron density profile have been presented, without derivation, in Ref. [13]. Employing similar procedures and the $\rho(r)$ function specified in Eq. (2), we have derived the two-dimensional SAXS amplitudes and the two-dimensional SAXS intensities of our tilted model track. Then, the latter quantities were integrated over ϕ. Integration was performed separately at the appropriate (pixel wide) adjacent intervals of θ covering one of the two identical mirror-like scattering branches (see Fig. 1). With this procedure, the four needed sequences of the theoretical track scattering cross sections, $\sigma_L(q_r)$, have been derived. These are given by

$$\sigma_L(q_r) = \frac{w\lambda L(\pi R^2 f\rho_o r_e)^2}{\sin\beta\sin\phi_o}\left[2s\frac{J_1(q_r R)}{q_r R} + (1-s)\exp(-q_r^2R^2/4)\right]^2 \tag{3}$$

where $r_e = 2.818 \times 10^{-13}$ cm is the electron scattering length at small scattering angles, $w = 1.50 \times 10^{-4}$ rad is the angular interval covered by the actual pixel width, $\lambda = 0.1542$ nm is the wavelength of the primary Cu K_α X-ray beam, ϕ_o is the local azimuthal scattering angle at which $q_z = 0$, and J_1 is Bessel function of first order. We have attributed the partially damped oscillations in the scattering yield (Fig. 2) to dispersion in the track radius. Evidence for dispersion has been presented in Refs. [10] and [14]. Thus, as in Ref. [7], the theoretical track scattering cross sections have been derived by integration of Eq. (3) over a Gaussian distribution of track radii.

5. ANALYSIS AND DISCUSSION

Our track model predicts that for tracks with a given radial electron density function, $\sigma_L(q_r)$ is linearly proportional to L (see Eq. (3)). This predicted behavior matches the present experimental data, so all four ion-irradiated samples contain tracks that are characterized by the same $\rho(r)$. Application of Eqs. (1) and (3) to the composite $N(q_r)$

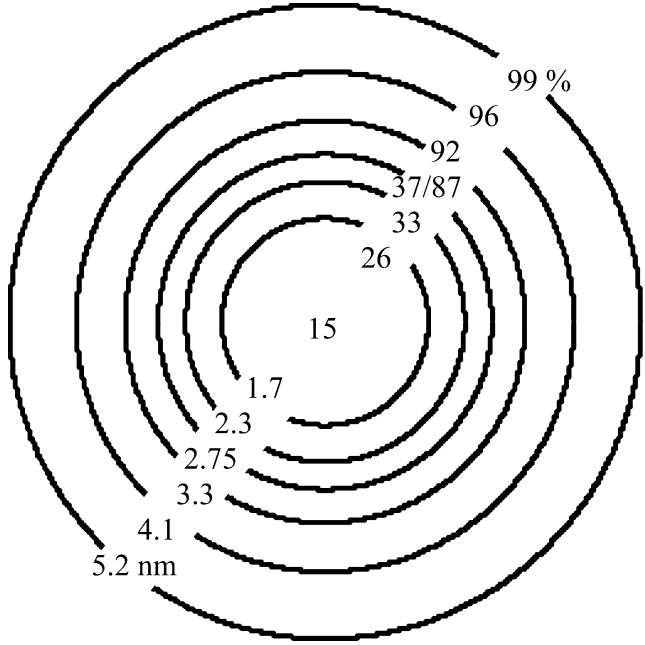

FIGURE 3 Residual electron density (percent of the matrix electron density) in the most probable track vs. the radial distance (in nm) from the track center.

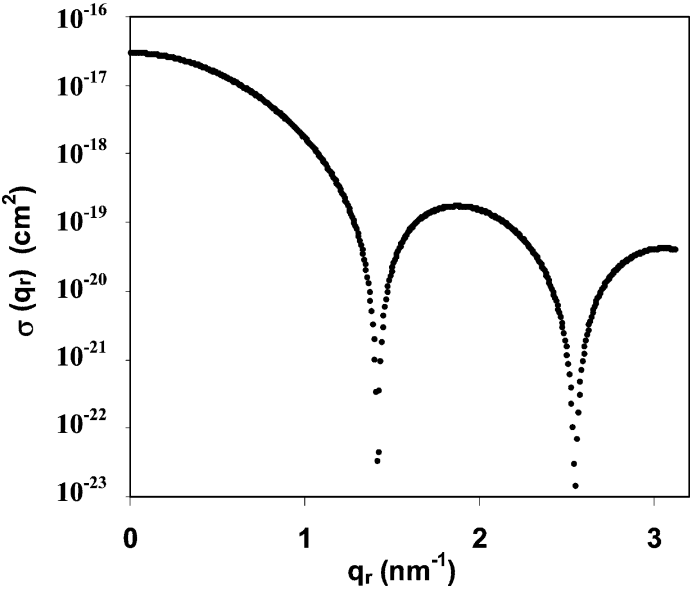

FIGURE 4 Theoretical SAXS cross sections of a 100-μm long track that is characterized by the most probable radial electron density distribution. The quantity q_r is the modulus of the radial component of the scattering vector in the reciprocal space.

sequence presented in Figure 2 has resulted in the theoretical scattering curve shown in Figure 2. This analysis gives a radial electron density profile that is 58% hard cylinder and 42% Gaussian ($s = 0.58$), a mean track radius of $R = 2.75 \pm 0.35$ nm, and fractional density deficit at the track center of $f = 0.85 \pm 0.08$. The most probable electron density distribution perpendicular to the track axis is displayed in Figure 3. The theoretical scattering cross sections of a track characterized by $L = 100\,\mu$m and the most probable $\rho(r)$ is displayed in Figure 4. Here, the highly oscillatory scattering pattern is governed by the abrupt change of electron density at a distance of 2.75 nm from the track center (see Fig. 3). Note that the morphology of 50-μm long U-ion tracks in polyimide (ion energy 2.64 GeV, LET 19.7 ± 0.5 keV/nm) has been characterized by $s = 0.58$, $R = 2.93 \pm 0.25$ nm, and $f = 0.64 \pm 0.06$ [7].

Assuming that the weighted mean electron density of residual track material is nearly similar to the electron density of the intact polymer, the ion-induced specific free volume along all presently examined tracks is $\sim 20\,\text{nm}^3$ per nm of track length. Thus, the process of track

formation undoubtedly involves material expulsion, most likely gas release. As argued in Ref. [7], only removal of gaseous and volatile molecules, most probably via permeation through the low-density tracks, could explain the necessary efficient transport of material from deep beneath the foil surface. Supportive experimental evidence for this process – gas release from polyimide under irradiation with Kr ions [15,16] – has been quoted in Ref. [7].

We attribute track porosity to a two-step process [7,8]. First, there is confined and intense ion-induced polymer degradation. Second, gaseous and volatile alteration products are released via permeation. Radiolysis can be initiated directly by the primary reactive species – released energetic electrons, ions, radicals, and excited molecular fragments – formed by the intense series of electron ionization, excitation, and dissociation events that occur during ion energy deposition (time scale 10^{-17} to 10^{-15} s). Creation of energized ions or atoms via Coulomb explosion events (ion spike scenario, time scale $\sim 10^{-13}$ s, see Ref. [17]) or delayed thermal agitation (thermal spike scenario, time scale 10^{-12} to 10^{-11} s, see Refs. [18] and [19]) is perhaps not necessary for initiation of radiolysis. We should also emphasize that these two frequently discussed track formation mechanisms cannot account for the newly discovered sizeable free volume in polymeric ion tracks (Refs. [7] and [8], and present article). Note, however, that the ion spike model and the thermal spike model may account for the hole structure of fresh very short ($\sim$ 50 nm long) tracks created in skybond (Monsanto) polyimide foils by penetrating 1.83 GeV Au ions, as observed by transmission electron microscopy (LET 15.4 keV/nm, mean track radius 4.0 ± 0.9 nm) [14]. If the released alteration products included energized nonvolatile fragments, it is possible that these species gained the necessary kinetic energy via Coulomb explosion or thermal spike events [14].

6. SUMMARY AND CONCLUSIONS

Four-month old latent tracks that were formed across 25, 50, 75, and 125 μm thick polyimide foils upon irradiation with penetrating 2.19 GeV Au ions (uniform LET of $\sim$15.5 keV/nm) possess, independent of the track length, uniform longitudinal specific free volume of about 20 nm^3 per nm of track length. Only highly-efficient release of gaseous and volatile alteration products, formed by intense ion-induced radiolysis, may explain the observed sizeable material loss. Free volume and high chemical reactivity of residual degradation products make ion tracks in polyimide especially suitable for track applications.

REFERENCES

[1] Fleischer, R. L., Price, P. B., & Walker, R. M. (1975). *Nuclear Tracks in Solids*. University of California Press: Berkeley, US.

[2] Spohr, R. (1990). *Ion Tracks and Microtechnology*. Vieweg: Braunschweig, Germany.

[3] Martin, C. R. (1994). Nanomaterials: A membrane-based synthetic approach. *Science*, *266*, 1961.

[4] Fert, A. & Piraux, L., (1998) Magnetic nanowires. *J. Magn. Magn. Mater.*, *200*, 338.

[5] Dobrev, D., Vetter, J., Neumann, R., & Angert, N. (2001). Conical etching and electrochemical metal replication of heavy-ion tracks in polymers foils. *J. Vac. Sci. Technol. B*, *19*, 1385.

[6] Toimil Molares, M. E., Hohberger, E. M., Schaeflein, Ch., Blick, R. H., Neumann, R., & Trautmann, C. (2003). Electrical characterization of electrochemically grown single copper nanowires. *Appl. Phys. Lett.*, *82*, 2139.

[7] Abu Saleh, S. & Eyal, Y. (2004). Porous tracks along wakes of swift uranium ions in polyimide. *Appl. Phy. Lett.*, *85*, 2529.

[8] Abu Saleh, S. & Eyal, Y. (2005). Morphology of track cores and halos created by swift uranium ions in polycarbonate. *Nucl. Instrum. Methods Phys. Res. B*, *236*, 81–87.

[9] Ferain, E. & Legras, R. (2003). Track-etch templates designed for micro- and nanofabrication. *Nucl. Instrum. Methods Phys. Res. B*, *208*, 115.

[10] Abu Saleh, S. & Eyal, Y. (2003). Observation of heavy-ion tracks in polyimide by means of high-resolution scanning electron microscopy. *Nucl. Instrum. Methods Phys. Res. B*, *208*, 137.

[11] Riedel, C. & Spohr, R. (1979). Statistical properties of etched nuclear tracks I. Analytical theory and computer simulation. *Radiat. Eff.*, *42*, 69.

[12] Vainshtein, B. K. (1966). *Diffraction of X-Rays in Chain Molecules*. Elsevier: Amsterdam, Netherlands.

[13] Albrecht, D. J. (1983). *Untersuchung der von Schweren Ionen in Dielektrika Erzeugten Defektstrukturen Mittels Kleinwinkelstreuung*, Report GSI-83-13, Gesellschaft für Schwerionenforschung: Darmstadt, Germany.

[14] Eyal, Y. & Gassan, K. (1999). Observation of latent heavy-ion tracks in polyimide by means of transmission electron microscopy. *Nucl. Instrum. Methods Phys. Res. B*, *156*, 183.

[15] Steckenreiter, T., Balanzat, E., Fuess, H., & Trautmann, C. (1999). Pyrolytic effects induced by energetic ions in polymers. *Nucl. Instrum. Methods Phys. Res. B*, *151*, 161.

[16] Steckenreiter, T., Balanzat, E., Fuess, H., & Trautmann, C. (1999). Chemical degradation of polyimide and polysulfone films under the irradiation with heavy ions of several hundred MeV. *J. Polym. Sci. Part A: Polym. Chem.*, *37*, 4318.

[17] Fleischer, R. L., Price, P. B., & Walker, R. M. (1965). Ion explosion spike mechanism for formation of charged-particle tracks in solids. *J. Appl. Phys.*, *36*, 3645.

[18] Chadderton, L. T. & Torrens, I. McC. (1969). *Fission Damage in Crystals*, Methuen: London, Great Britain.

[19] Toulemonde, M., Dufour, C., & Paumier, E. (1992). Transient thermal process after a high-energy heavy-ion irradiation of amorphous metals and semiconductors. *Phys. Rev. B*, *46*, 14362.